POSITION AND ORIENTATION MEASUREMENT FOR AUTONOMOUS AERIAL REFUELING BASED ON MONOCULAR VISION

Wenqi Wu, Xingang Wang, De Xu, and Yingjie Yin

Abstract

Combined with the 3D model of aerial refueling drogue target, this paper proposes a method for measuring the position and orientation based on monocular vision. The shape of the drogue's inner dark part is circular and its image is a circle or an ellipse in the image space. The contour points of the dark part are extracted in the image space and the adaptive elliptical parameter extraction algorithm based on RANSAC is adopted to get the parameters of the ellipse in the image space. Based on the principle of pinhole imaging and the dimension of the drogue's dark part, a visual cone is established and the position and orientation of the drogue's inner dark part can be deduced by using the geometric relationships. The experiments for measuring the drogue's position and orientation are carried on in a platform composed of two KUKA robots, and the experiment results verify the effectiveness of the proposed method.

Key Words

Ellipse fitting, Position and orientation measurement, Monocular vision, Aerial refueling

1. Introduction

Research Center of Precision Sensing and Control, Institute of Automation, Chinese Academy of Sciences, Beijing, China; email: {Wenqi Wu, wuwenqi2013@ia.ac.cn}, {Xingang Wang, xingang.wang@ia.ac.cn}, {De Xu, de.xu@ia.ac.cn}, {Yingjie Yin, yingjie.yin@ia.ac.cn}
Manuscript received 14 June 2015

Aerial refueling is used to add fuel to in-flight aircraft and it is very important for improving the aircraft's endurance and extending cruising mileage. As shown in Fig.1, the aerial refueling system is mainly composed of a drogue dragged by the front refueling aircraft (the tanker) and a probe on another aircraft (the receiver) in the rear of the tanker. The key of aerial refueling is the accurate docking of the probe and drogue in the air. At present, most aircraft refueling process is completed by the manual operation, and the operation is difficult. As the urgent demand for the aerial refueling of UAVs [1-8], how to achieve automatic aerial refueling become very important. Visual measurement method is widely used in automatic aerial refueling [9-12]. John Valasek *et al*. designed vision-based sensors and navigation systems [9]. The device comprises two parts, one is a sensor installed in the receiver aircraft for sensing location information, the other is LED beacons installed in the refueling drogue. The disadvantage of this method is the need to modify the structure of the drogue and adding auxiliary devices. Fravolini *et al*. [10] achieved the position and orientation measurement of the drogue by combining GPS information and visual information. The GPS information is used to measure the relative position between the receiver aircraft and the tanker. The visual information is used to measure the relative position and orientation between the camera and drogue. Carol Martinez *et al*. [11] used monocular vision to achieve the detection, tracking and measuring drogue targets. The circumscribed rectangle of the drogue target is detected and tracked to realize the drogue center position measurement in the camera coordinate system based on P4P (Perspective-4-point) approach. However, this method cannot correctly measure the drogue’s orientation and it will produce large measurement error when the angle between drogue plane and optical axis of the camera is large because the circumscribed rectangle’s four corner points in the image space cannot always match the same group of four specified points in Cartesian space.

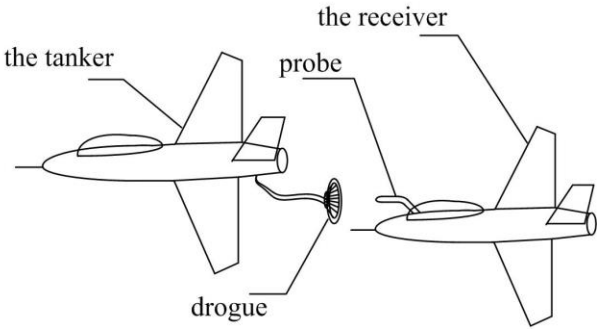

Figure 1. Aerial refueling system

By aid of the drogue's model information, this paper proposes a method for measuring the drogue's position and orientation based on monocular vision [12]. The perspective projection model shows that, when the drogue target is perpendicular to the optical axis of the camera, its image is a circle on the image plane. However, in most cases the image is an ellipse because the drogue target is not perpendicular to the optical axis of the camera. In previous work [13], we propose a detection and tracking method based on the shape of the drogue and it can effectively locate the position of contour points of the drogue's inner dark part in the image space. This paper uses self-adaptive least squares method based on RANSAC to fit the ellipse's parameters from the contour points set detected by [13] and then adopts parameter clustering to find the optimal estimation model to improve the adaptability of the algorithm. Our approach refers the visual measurement model in [14-18] to construct position and orientation measurement model based on the model of drogue target. A virtual camera coordinate system in the visual cone of the visual measurement model is set up, and the drogue position and orientation is deduced in the virtual camera coordinate system. By using the coordinates conversion relation between real and virtual camera coordinate system, the real position and orientation of drogue target can be deduced. The experiments for measuring the drogue's position and orientation are carried on in a platform composed of two KUKA robots, and the experiment results verify the effectiveness of our proposed method.

2. Adaptive Elliptical Parameter Extraction Algorithm Based on RANSAC

2.1 The least squares fitting ellipse

In the two-dimensional plane coordinate system, the general form of the equation for an ellipse is:

$$A_e x^2 + B_e xy + C_e y^2 + D_e x + E_e y + F_e = 0 \tag{1}$$

The optimization goal of the ellipse fitting is to minimize the sum of squared distances from the sample point to the ellipse to get the minimum value of the objective function f_o:

$$f_o = \sum_{i=1}^{n} (A_e x_i^2 + B_e x_i y_i + C_e y_i^2 + D_e x_i + E_e y_i + F_e)^2 \tag{2}$$

where n is the number of sample points. The constraint $A+C=1$ is added to avoid zero solution and multiple solutions [19]. A system of linear equations can be obtained by setting the objective function's partial derivatives with respect to parameters A_e, B_e, C_e, D_e, E_e and F_e, and the parameters of general elliptic equation can be obtained by solving the system of linear equations. If the results satisfy $B_e^2-4A_eC_e<0$, then an ellipse is obtained; Otherwise, discard the results. To describe the geometric characteristics of the ellipse, it is necessary to know the geometry parameters of the ellipse, which are the center coordinates of ellipse (x_e, y_e), major axis a_e, minor axis b_e and rotation angle θ_e. The geometrical parameters of ellipse can be obtained by equation (3)-(7):

$$x_e = \frac{B_e E_e - 2C_e D_e}{4A_e C_e - B_e^2} \tag{3}$$

$$y_e = \frac{B_e D_e - 2A_e E_e}{4A_e C_e - B_e^2} \tag{4}$$

$$a_e = 2\sqrt{\frac{-2F_e}{A_e + C_e - \sqrt{B_e^2 + \left(\frac{A_e - C_e}{F_e}\right)^2}}} \tag{5}$$

$$b_e = 2\sqrt{\frac{-2F_e}{A_e + C_e + \sqrt{B_e^2 + \left(\frac{A_e - C_e}{F_e}\right)^2}}} \tag{6}$$

$$\theta_e = \frac{1}{2}\arctan\frac{B_e}{A_e - C_e} \tag{7}$$

2.2 RANSAC algorithm and clustering algorithm

The core idea of RANSAC algorithm is to find the optimal model in the random sampling process. A small amount of points are utilized to estimate the model, and the surplus sample points are used to verify the estimation model. As a result, all of the sample points, corresponding to the estimation model, are added into the agree set. When the number of samples in the agree set of an estimation model is greater than the threshold N_T, The final parameters of ellipse model are obtained by the least squares fitting of the data in the agree set. The adaptability of the threshold is poor when the data are subjected to noise interference, so we use clustering method to analyze the ellipse parameters set to achieve an adaptive threshold selection. The ellipses are fitted with the random sampling points. Then, the clustering analysis on parameters of ellipse is executed. The cluster center which contains the most sample points and owns the highest density is regarded as the parameters of correct estimation model.

In order to obtain the correct estimation of ellipse, agglomerate hierarchical clustering algorithm is used to analyze the ellipse parameters set. Here are two groups of elliptical parameter vectors $V_i=(x_{ei},y_{ei},a_i,b_i,\theta_i)$, $V_j=(x_{ej},y_{ej},a_j,b_j,\theta_j)$, the distance between them is defined as:

$$d_d(V_i,V_j) = \sqrt{\begin{aligned}&(x_{ei}-x_{ej})^2+(y_{ei}-y_{ej})^2+(a_{ei}-a_{ej})^2\\&+(b_{ei}-b_{ej})^2+(\theta_{ei}-\theta_{ej})^2\end{aligned}} \tag{8}$$

Agglomerate hierarchical clustering algorithm is used in the ellipse parameter space containing N groups of parameters. Firstly, each parameter is denoted as a category n_i, the number of samples contained in n_i is denoted as m_i, cluster centers is denoted as P_i, then the between-class distance matrix can be initialized as the product of distance matrix between each category and distance matrix between cluster centers:

$$\begin{aligned}D_d &= [d_d(n_i,n_j)]_{N\times N}\times[d_d(P_i,P_j)]_{N\times N}\\ &1\le i\le N, 1\le j\le N\end{aligned} \tag{9}$$

The classes n_i and n_j whose between-class distance is minimum are merged into a new class n_{inew}, and the new cluster center is:

$$P_{inew} = \frac{(P_i \times m_i + P_j \times m_j)}{m_i + m_j} \tag{10}$$

Then the *jth* row and *jth* column of the between-class distance matrix are deleted and the value of the *ith* row and *ith* column of the between-class distance matrix are updated according to the new cluster center P_{inew}. The clustering continues until the minimum of between-class distance is greater than the threshold *T*. The center of clustering of every class and the number of samples corresponding to the class are obtained by the agglomerate hierarchical clustering algorithm. The cluster center, have maximum number of samples, is regarded as the correct parameters estimation of ellipse.

2.3 Adaptive elliptical parameter extraction algorithm

The integral process of RANSAC-based adaptive elliptical parameter extraction is presented in Algorithm 1. The sample set *P* and the geometrical parameters of ellipse are regarded as the input and output of Algorithm 1, respectively.

Algorithm 1: RANSAC-based adaptive elliptical parameter extraction

Input: the sample set *P*
Output: fitted elliptical parameter $\boldsymbol{x_e, y_e, a_e, b_e, \theta_e}$
1 **for** $k = 1$ **to** N **do**
2 Randomly select n sample points and add in sub-sample set P_s
3 Least squares fitting get $x_{ek}, y_{ek}, a_{ek}, b_{ek}, \theta_{ek}$
4 $x_{ek}, y_{ek}, a_{ek}, b_{ek}, \theta_{ek}$ add in the ellipse parameters set *S*
5 **end**
6 Compute the distance between two elliptical parameter vectors $d_d(V_i, V_j)$ using equation (8)
7 initialize the between-class distance matrix D_d
8 **for** $k = 1$ **to** N-1 **do**
9 **for** $k = 1$ **to** N **do**
10 Compute D_d between n_i and n_j
11 **end**
12 Merge n_i and n_j whose min(D_d) to form a new class n_{inew}
13 Get the new cluster center P_{inew}

13 Update D_d
14 **if** minimum($d_d(V_i,V_j)$) < threshold T **then**
15 Get the correct estimation of ellipse M^* and Stop loop circle
16 **end**
17 **end**
18 Compute deviation b_s between M^* and the sample in P to find the effective edge points set P^*
19 Using least squares fitting on P^* to get x_e,y_e,a_e,b_e,θ_e
20 **Return** $\boldsymbol{x_e,y_e,a_e,b_e,\theta_e}$

The steps for adaptive elliptical parameter extraction algorithm based on RANSAC and clustering analysis of parameter space are as follows. Firstly, the sampling number is set to N, a sub-sample set P_s containing n sample points is randomly selected in the sample set P and n ≥ 5, which is the minimum quantity of points for fitting ellipse. The method of least squares fitting is used to get the parameters of ellipse. Then the process of random selection of sample subsets and fitting ellipse parameters extraction is repeated to get the ellipse parameters set S. Then cluster analysis was performed on the ellipse parameters set in the parameter space and the clustering center contains the most sample categories is the correct parameters estimation of ellipse M^*. Finally, the deviation estimation method is used to get the effective edge points set P^*, and calculate the deviation b between the samples in sample set P and the correct estimation of ellipse M^*. All sample points whose deviations are less than the threshold compose the effective edge points set P^*. The final ellipse can be obtained by using least squares fitting on P^*.

The multi-group parameters are calculated by the multi-times random sampling in extensive experiments, and the result of these experiments expresses the phenomenon which is the parameters assembled around the parameters of correct estimation model. Therefor the cluster center which contains the most sample points and owns the highest density is regarded as the parameters of correct estimation model. In the meantime, the convergence of the proposed algorithm is decided by the clustering algorithm. Since the agglomerate hierarchical clustering algorithm itself possess high convergence, can be found in [20], and the convergence of the proposed Algorithm 1 can be guaranteed similarly.

3. Position and Orientation Measurement for Drogue Target

3.1 Visual measurement principle

The projection of the inner circular dark part of drogue target in a different position and orientation is an ellipse in the image plane. The visual measurement principle from the drogue target to the image plane is shown in Fig.2.

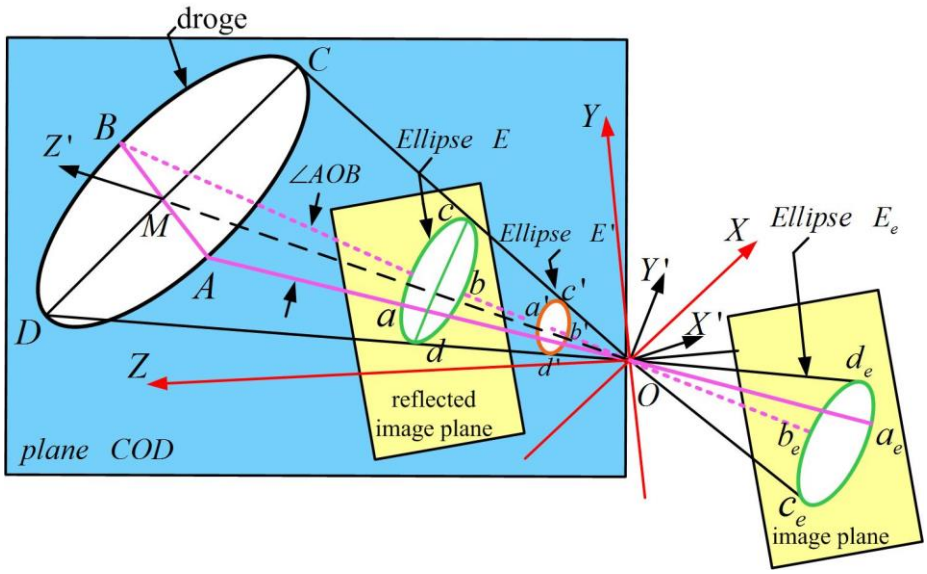

Figure 2. Visual measurement principle

In Fig.2, the camera optical center O and the axes X, Y, Z stand for real camera coordinate system. The image of the inner circular dark part (represented as ABCD in Fig.2) of drogue target in the image plane is the ellipse E_e, that is fitted by the effective edge points set P^*. By the inverse perspective projection, the image plane can be reflected in the positive direction of Z axis of the camera coordinate system and the ellipse E in the reflected image plane corresponds to the ellipse E_e in the image plane. A visual cone structure is composed of the camera optical center O, ellipse E and inner circular dark part of drogue target $ABCD$. The angle $\angle AOB$ is the maximum angle, which is constructed by point O and any two points on ellipse E. These two points on the ellipse E are defined as a and b. The extension lines of Oa and Ob on visual cone intersect the ellipse internal circular dark part at points A and B. There is the angular bisector

of $\angle AOB$, which intersects chord *AB* at point *M*. Then the plane *COD* which contains the line *OM* and is perpendicular to plane *AOB* is constructed. The plane *COD* intersects circular dark part of drogue at points *C*, *D* and the ellipse *E* at points *c*, *d*. Besides, a virtual camera coordinate system is established and *OM* is the z-axis of the virtual camera coordinate system. The z-axis is presented as *Z'* in Fig.2 and can be expressed as the unit vector $\overline{z'}$:

$$\overline{z'} = (\overrightarrow{uOA} + \overrightarrow{uOB}) / \left| \overrightarrow{uOA} + \overrightarrow{uOB} \right| \tag{11}$$

where $\overrightarrow{uOA}$ and $\overrightarrow{uOB}$ are unit vectors. The virtual y-axis is defined as *Y'* and is perpendicular to the plane *AOB*, which can be expressed as the unit vector $\overline{y'}$:

$$\overline{y'} = (\overrightarrow{uOA} \times \overrightarrow{uOB}) / \left| \overrightarrow{uOA} \times \overrightarrow{uOB} \right| \tag{12}$$

The virtual x-axis is defined as X' and is perpendicular to the plane composed of $\overline{y'}$ and $\overline{z'}$, which can be expressed as the unit vector $\overline{x'}$:

$$\overline{x'} = \overline{z'} \times \overline{y'} \tag{13}$$

Thus, a virtual camera coordinate system *X'Y'Z'* can be constructed and the geometric relations are established in the virtual camera coordinate system. In the coordinate system *X'Y'Z'*, a virtual image plane which is perpendicular to the *Z'*-axis is constructed. The distance along the *Z'*-axis between the virtual image plane and the camera optical center *O* is the focal length *f*, and this virtual image plane can be intercepted by a visual cone to a virtual ellipse *E'*. This virtual ellipse *E'* intersects lines *OA*, *OB*, *OC* and *OD* at points *a'*, *b'*, *c'* and *d'* respectively on the visual cone. Accordingly, the geometric relationships between inner circular dark part *ABCD* of drogue, ellipse *E* and virtual ellipse *E'* in the visual cone is established.

3.2 Position and orientation measurement model

As shown in Fig.3, the ellipse *E'* is projected onto the plane *X'OY'* in the virtual camera coordinate

system *X'Y'Z'*.

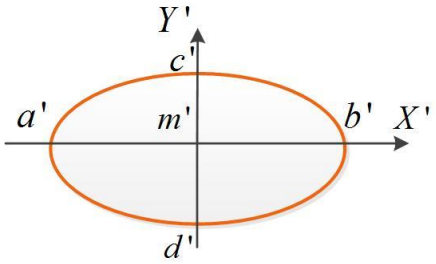

Figure 3. Virtual ellipse *E'*

m' shown in Fig.3 is the intersection of *Z'*-axis and ellipse *E'* and it is also the ellipse center, so *a'b'* and *c'd'* are the long axis and short axis of the ellipse respectively. Therefore, $a'=(l_{a'},0,f)$, $b'=(-l_{b'},0,f)$, $c'=(0,l_{c'},f)$ and $d'=(0,-l_{d'},f)$ can be deduced within the cone constituted by camera optical center *O* and the ellipse *E'*. $l_{a'}$, $l_{b'}$, $l_{c'}$ and $l_{d'}$ can be obtained by equations (14) and (15).

$$l_{a'} = l_{b'} = f\tan(\angle a'Ob'/2) \tag{14}$$

$$l_{c'} = l_{d'} = f\tan(\angle c'Od'/2) \tag{15}$$

$l_{a'}$ and $l_{b'}$ are the length of virtual elliptical semi-major axis, $l_{c'}$ and $l_{d'}$ are the length of virtual elliptical semi-minor axis. The representation *A*, *B*, *C*, *D* can be obtained by the geometric properties of visual cone:

$$A = \gamma a' = (\gamma l_{a'}, 0, \gamma f) \tag{16}$$

$$B = \gamma b' = (-\gamma l_{b'}, 0, \gamma f) \tag{17}$$

$$C = \alpha c' = (0, \alpha l_{c'}, \alpha f) \tag{18}$$

$$D = \beta d' = (0, -\beta l_{c'}, \beta f) \tag{19}$$

Where γ is the proportion coefficient between *a'* and *A*, *b'* and *B*, α is the proportion coefficient between *c'* and *C*, β is the proportion coefficient between *d'* and *D*. The virtual center of inner circular dark part of drogue *F'* is:

$$F' = (C+D)/2 = (0, l_{c'}(\alpha-\beta)/2, (\alpha+\beta)f/2) \tag{20}$$

Where *r* is set to real radius of inner circular dark part of drogue. The equation (21) is obtained by the

properties of the circle and the geometric equivalent relations.

$$\begin{cases} |\overline{F'A}| = |\overline{F'B}| = r \\ |\overline{F'C}| = |\overline{F'D}| = r \\ |\overline{OC}| / |\overline{OD}| = |\overline{CM}| / |\overline{DM}| \end{cases} \tag{21}$$

In the virtual camera coordinate system *X'Y'Z'*, the solution of the proportion coefficient α, β and γ are calculated by the equation (21), and the expression of α, β and γ are deduced as:

$$\begin{cases} \alpha = \dfrac{r}{l_{a'}}\{[\dfrac{(l_{a'}{}^2 + f^2)}{(l_{c'}{}^2 + f^2)}]^{\frac{1}{2}} + [\dfrac{(l_{a'}{}^2 - f^2)}{(l_{c'}{}^2 + f^2)}]^{\frac{1}{2}}\} \\ \beta = \dfrac{r}{l_{a'}}\{[\dfrac{(l_{a'}{}^2 + f^2)}{(l_{c'}{}^2 + f^2)}]^{\frac{1}{2}} - [\dfrac{(l_{a'}{}^2 - f^2)}{(l_{c'}{}^2 + f^2)}]^{\frac{1}{2}}\} \\ \gamma = \dfrac{r}{l_{a'}}[\dfrac{(l_{a'}{}^2 + f^2)}{(l_{c'}{}^2 + f^2)}]^{\frac{1}{2}} \end{cases} \tag{22}$$

From above equations, the center coordinate *F'* and normal vector $\vec{n}'$ can be represented as equation (23) and (24), respectively.

$$F' = (0, \frac{rl_{c'}}{l_{a'}}\sqrt{\frac{l_{a'}^2 - l_{c'}^2}{l_{c'}^2 + f^2}}, \frac{rf}{l_{a'}}\sqrt{\frac{l_{a'}^2 + f^2}{l_{c'}^2 + f^2}}) \tag{23}$$

$$\vec{n}' = \frac{\overline{AB} \times \overline{CD}}{|\overline{AB} \times \overline{CD}|} = \frac{(0, \sqrt{l_{a'}^2 - l_{c'}^2} f, -\sqrt{l_{a'}^2 + f^2} l_{c'}^2)}{\sqrt{(l_{a'}^2 - l_{c'}^2) f^2 + (l_{a'}^2 + f^2) l_{c'}^2}} \tag{24}$$

F and $\vec{n}$ are set to, respectively, the center coordinate and normal vector of the inner circular dark part of drogue in a real camera coordinate system. The rotation matrix between coordinate system *Z'* and coordinate system *Z* can be derived by conversion relations shown in Fig.4. *F'* and $\vec{n}'$ are converted to *F* and $\vec{n}$ by equations (25), (26) and (27).

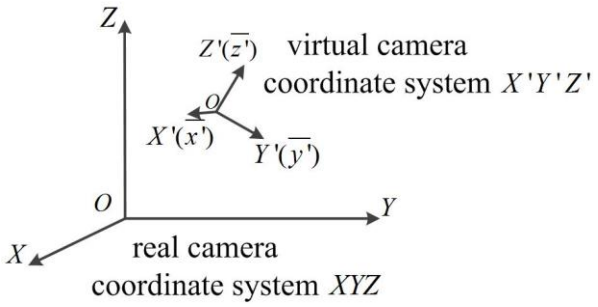

Figure 4. Coordinate system conversion

$$ {}^{Z}_{Z'}R = [{}^{Z}_{Z'}x, {}^{Z}_{Z'}y, {}^{Z}_{Z'}z] = [\overline{x'}, \overline{y'}, \overline{z'}] \tag{25} $$

$$ {}^{Z}F = {}^{Z}_{Z'}R\,{}^{Z'}F' \tag{26} $$

$$ {}^{Z}\vec{n} = {}^{Z}_{Z'}R\,{}^{Z'}\vec{n} \tag{27} $$

Where ${}^{Z}_{Z'}R$ represents the rotation matrix from *Z'* coordinate system to Z coordinate system.

4. Experimental Results

The experiment was divided into two parts. The first part was the ellipse fitting experiment. RANSAC-based adaptive ellipse fitting method proposed was compared with random ellipse detection based on Hough transform [21] and fixed threshold ellipse parameters fitting based on RANSAC [22]. The second part was the experiment of the drogue target's position and orientation measurement. We collected 10 data of drogue target in different positions and orientation. The proposed method was compared with the method proposed by Carol Martinez *et al.* [11].

4.1 Experimental Platform and KUKA Robot Group Measurement Process

As shown in Fig.5, the experimental platform was composed of two KUKA robots, drogue, probe and camera. The camera was Basler acA1300 30gm/gc, the focal length of this camera is 5 mm and the resolution of each image acquisition is 1280×960 pixels.

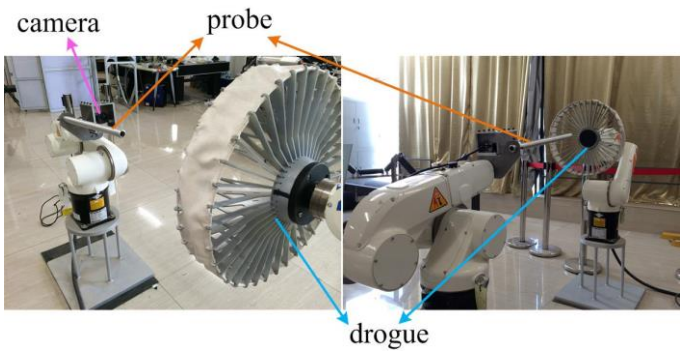

Figure 5. Actual picture of KUKA experiment platform

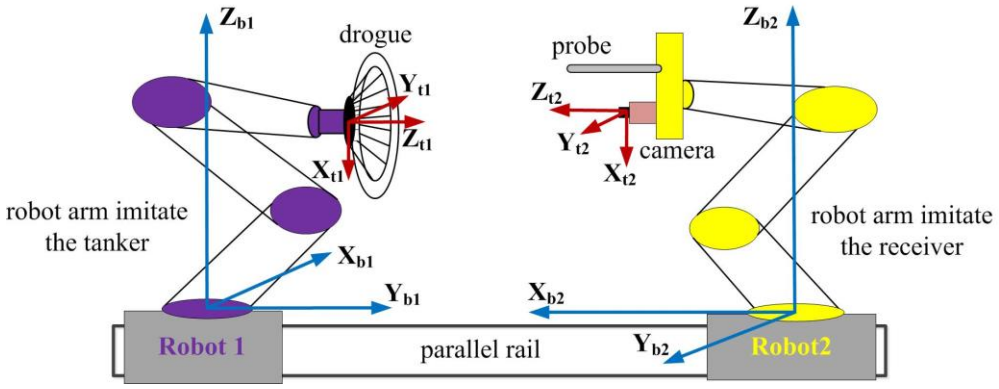

Figure 6. Schematic diagram of KUKA experiment platform

Schematic diagram of experimental platform is shown in Fig.6, drogue target was installed on the end of the robot 1, the probe and the camera was installed on the end of the robot 2 to simulate receiver aircraft. Four coordinate systems {$t1$}, {$t2$}, {$b1$} and {$b2$} were built in the two robots in Fig.6. Among them, {$t1$} and {$t2$} coordinate systems were the tool coordinate systems of robot 1 and robot 2 respectively, {$b1$} and {$b2$} coordinate systems were the base coordinate systems of robot 1 and robot 2. The conversion relations between {$t1$} and {$b1$}, {$t2$} and {$b2$} were established through the transformation matrix. Then the Flange calibration method was used for determination of the conversion relationship between {$b1$} and {$b2$}.

$$P_{b1}=\begin{bmatrix} {}^{b1}p_1 & {}^{b1}p_2 & \cdots & {}^{b1}p_n \\ 1 & 1 & \cdots & 1 \end{bmatrix}_{4\times n} \tag{28}$$

$$P_{b2}=\begin{bmatrix} {}^{b2}p_1 & {}^{b2}p_2 & \cdots & {}^{b2}p_n \\ 1 & 1 & \cdots & 1 \end{bmatrix}_{4\times n} \tag{29}$$

$${}^{b2}T_{b1}=\begin{bmatrix} {}^{b2}R_{b1} & {}^{b2}p_{b1} \\ 0 & 1 \end{bmatrix}_{4\times 4} \tag{30}$$

where P_{b1} and P_{b2} are matrixes which consist of point coordinates in coordinates system {$b1$} and {$b2$} coordinates respectively. ${}^{b2}T_{b1}$ is the transformation matrix from coordinates {$b1$} to coordinates {$b2$},

${}^{b2}R_{b1}$ is the orientation rotation matrix from coordinates $\{b1\}$ to coordinates $\{b2\}$ and ${}^{b2}P_{b1}$ is the position vector from coordinates $\{b1\}$ to coordinates $\{b2\}$.

$$P_{b2}={}^{b2}T_{b1}P_{b1} \tag{31}$$

$${}^{b2}T_{b1} = P_{b2}P_{b1}^{T}(P_{b1}P_{b1}^{T})^{-1} \tag{32}$$

As shown in the equation (32), the least squares fitting method was used to get the coordinate transformation matrix ${}^{b2}T_{b1}$ and the conversion relationship between the coordinate system $\{b1\}$ and $\{b2\}$. When ${}^{b2}T_{b1}$ was obtained, the equation (31) was used to get the coordinate representation of any point on the edge of the drogue inner circular dark part of robot 1 in robot 2's camera coordinate system. As the actual radius of inner circular dark part of drogue was known, we represented the center coordinates of the drogue inner circular dark part and the coordinates of edge points in robot 2's camera coordinate system by using conversion relations between the coordinate systems. Normal vector was fitted with edge points, thus the position and orientation were used to compare with the results which were obtained by visual method.

4.2 Ellipse Fitting Experiment

The result of ellipse fitting experiment as shown in Fig.7, (a) is a physical image, (b), (c), (d) are the results of ellipse fitting by using three methods respectively. Among them, (b) is the method used in this paper, (c) is random ellipse detection method and (d) is fixed threshold ellipse parameters fitting based on RANSAC method.

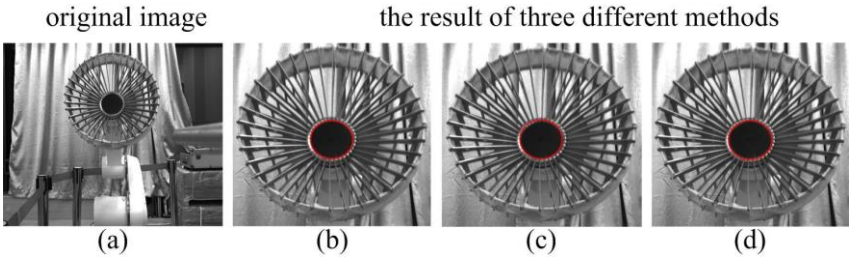

Figure 7. Experiment result of ellipse fitting

Three ellipse fitting methods above were used to get 10 images of arbitrary position and orientation of drogue target under the same conditions of continuous motion as shown in Fig.8. After 10 groups of experiments, we got the center coordinates of ellipse fitting, semi-major axis, semi-minor axis and rotation angle, and their average errors between the actual ellipse five parameters were represented as $\overline{e}_{x_e}$, $\overline{e}_{y_e}$, $\overline{e}_a$, $\overline{e}_b$ and $\overline{e}_\theta$ as shown in Table 1. It can be seen that our ellipse fitting method was better than others.

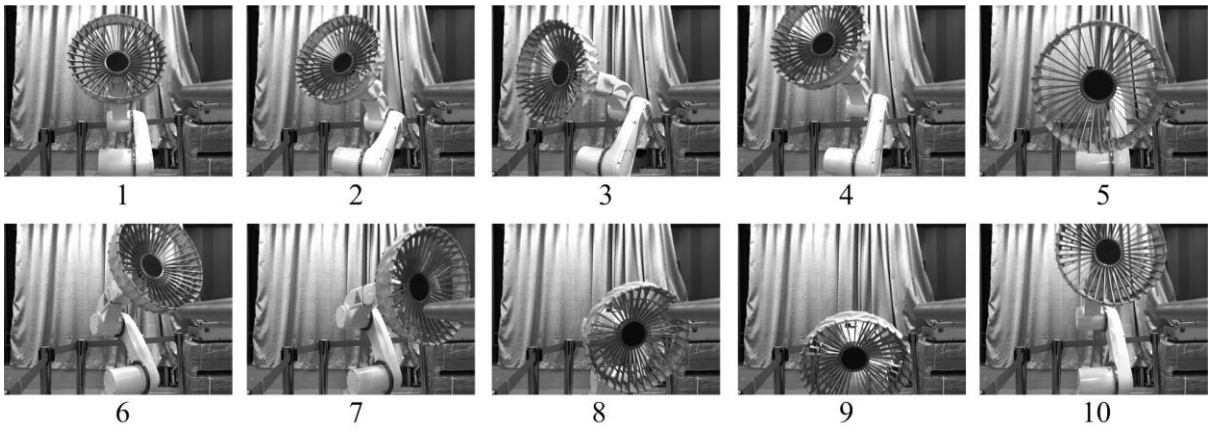

Figure 8. Different position and orientation of the drogue target

Table 1
Average error of ellipse fitting

	$\overline{e}_{x_e}$ (pixel)	$\overline{e}_{y_e}$ (pixel)	$\overline{e}_a$ (pixel)	$\overline{e}_b$ (pixel)	$\overline{e}_\theta$ (deg)
The proposed method in this paper	1.2	1.3	1.4	1.3	3.4
Random ellipse detection method [21]	6.2	5.9	5.7	6.2	8.5
Fixed threshold based RANSAC method [22]	2.7	2.7	2.5	2.2	6.7

4.3 Experiment Result of Position and Orientation Measurement of Drogue Target

The position and orientation, were measured by KUKA robots group, of the first experiment were considered as benchmark (as shown in Fig.8). Then the measured offsets from the benchmark to the measurement values of the second to tenth experiments with the proposed method and the method in [11] were computed. They were compared with the actual offsets obtained by KUKA robot. In the position measurement, the point coordinate of the drogue internal circle in 3D space was used as the position, the offset was defined as the distance between two points in the x, y, z-axis and expressed as Δx, Δy and Δz. In

the orientation measurement, normal vector of the drogue inner circular dark park was used as the orientation, the offset was defined as the angle between two normal vectors and expressed as deviation angle $\Delta\theta$. Position measurement results are shown in Table 2, orientation measurement results are shown in Table 3.

Table 2
Experimental results of position measurement

		1	2	3	4	5	6	7	8	9
Actual value	Δx (mm)	0.39	62.80	75.47	116.90	44.66	55.64	235.42	334.13	86.81
	Δy (mm)	92.78	188.04	131.88	18.43	146.07	215.99	108.61	11.23	62.13
	Δz (mm)	59.67	104.74	23.77	300.52	102.13	215.87	135.18	120.34	161.47
Measured value with Our method	Δx (mm)	5.09	64.48	80.96	117.91	37.69	60.64	243.19	326.21	81.98
	Δy (mm)	94.90	189.97	136.93	17.88	143.24	211.94	104.93	10.56	58.34
	Δz (mm)	53.73	112.82	18.04	308.65	108.54	222.76	144.14	127.61	156.98
Measured value with the method in [11]	Δx (mm)	15.61	69.48	61.05	115.71	40.73	45.31	252.51	344.48	75.43
	Δy (mm)	83.00	167.90	110.88	19.22	114.33	183.74	95.07	12.56	59.44
	Δz (mm)	46.74	118.39	31.09	310.60	110.50	194.08	143.59	108.65	145.03

Table 3
Experimental results of orientation measurement

		1	2	3	4	5	6	7	8	9
Actual value	$\Delta\theta$ (deg)	53.09	61.40	49.52	32.19	37.00	65.52	83.79	69.96	8.66
Measured value with Our method	$\Delta\theta$ (deg)	54.16	61.15	46.31	31.36	36.14	63.94	85.22	68.79	9.00

The results of the first to ninth group in Table 2 and Table 3, respectively correspond to the second to tenth images in Fig.8. The results (shown in Table 2) of our method show that the offsets between measured position and benchmark position obtained by the method proposed in this paper were more close to the actual offsets than that of Carol Martinez's method. In groups of 4, 8 and 9 experimental results (as shown in Table 2), the measured offsets were very close to the actual offsets and we can see from Fig.8 that the three images of drogue's orientation were similar to facing the camera. In other experiments the drogue's orientation changed a lot, so the method of Carol Martinez et al. had relatively large errors, and the errors would increase with increasing amplitude variations. Because of the position measurement

results carried by Carol Martinez *et al.* in the image space were depended on the drogue external rectangle and pinhole imaging model, the large measurement error was produced when the drogue orientation relative to the optical axis of the camera had a larger change. In the method proposed in this paper, the measurement results of the drogue in a different position and orientation had good stability. At the same time, the proposed method can also simultaneously measure the drogue orientation. We can conclude from Table 3 that the actual and measured deviation angles were very close. Therefore our method had good accuracy.

5. Conclusion

For aerial refueling tasks, we use monocular vision achieve 3-D space position and orientation measurement of the drogue targets. On the basis of accurately position the contour points of drogue's inner circle dark part in the image space, the adaptive elliptical parameter extraction algorithm based on RANSAC is used to get the parameters of the ellipse in the image space and the elliptical parameter space cluster analysis method is adopted to find the optimal parameters of the ellipse. This method improves adaptability and robustness of the ellipse fitting. Visual measurement model is established from the image plane to the drogue target, and the center coordinates of the drogue inner circular dark part and normal vector is deduced in the camera coordinate system. The experimental platform of two KUKA robots is adopted and the offsets of each set of experiments are compared with the benchmark to verify the effectiveness of the proposed method. Experimental results show that the proposed method can accurately measure the drogue target in different positions and orientations.

Acknowledgements

This work is partly supported by The National Natural Science Foundation of China (Grant No.

61421004), The National Natural Science Foundation of China (Grant No. 61573349), The National High Technology Research and Development Program of China (863 Program) (Grant No. 2015AA042308) and The Innovation Fund Project of the Chinese Academy of Sciences (Grant No. CXJJ-14-M08).

References

[1] M. Mammarella, G. Campa, M.R. Napolitano et al, Machine vision/GPS integration using EKF for the UAV aerial refueling problem, *IEEE Transactions on Systems, Man, and Cybernetics*, *38*(6), 2008, 791-801.

[2] R.V. Dellaquila, G. Campa, M.R. Napolitano et al. Real-time machine vision-based position sensing system for UAV aerial refueling, *Journal of Real-Time Image Processing*, *1*(3) 2007, 213-224.

[3] T.E. Speer, Systems and methods for automatically and semiautomatically controlling aircraft refueling, *The Boeing Company, US Patent*, 2008, 7469863.

[4] W.R. Williamson, G.J. Glenn, V.T. Dang et al, Sensor fusion applied to autonomous aerial refueling, *Journal of Guidance, Control, and Dynamics*, *32*(1), 2009, 262-275.

[5] M.L. Fravolini, M. Mammarella, G. Campa et al, Machine vision algorithms for autonomous aerial refueling for UAVs using the USAF refueling boom method, *Innovations in Defence Support Systems–1*, *304*, 2010, 95-138.

[6] K. Ro, J.W. Kamman, Modeling and simulation of hose-paradrogue aerial refueling systems, *Journal of Guidance, Control, and Dynamics*, *33*(1), 2010, 53-63.

[7] Z.H. Zhu, S.A. Meguid, Modeling and simulation of aerial refueling by finite element method, *International Journal of Solids and Structures*, *44*(24), 2007, 8057-8073.

[8] H.J. Asl, G. Oriolo, H. Bolandi, An adaptive scheme for image-based visual servoing of an underactuated UAV, *International Journal of Robotics and Automation*, *29*(1), 2014.

[9] J. Valasek, K. Gunnam, J. Kimmett et al, Vision-based sensor and navigation system for autonomous air refueling, *Journal of Guidance, Control, and Dynamics*, *28*(5), 2005, 979-989.

[10] M.L. Fravolini, A. Ficola, G. Campa et al, Modeling and control issues for autonomous aerial refueling for UAVs using a probe-drogue refueling system, *Aerospace Science and Technology*, *8*(7), 2004, 611-618.

[11] C. Martinez, T. Richardson, P. Thomas et al, A vision-based strategy for autonomous aerial refueling tasks, *Robotics and Autonomous Systems*, *61*(8), 2013, 876-895.

[12] J.P. Hsiao, S.S. Yeh, P.L. Hsu, Target postion estimation using multi-vision system implemented on destributed mobile robots, *International Journal of Robotics and Automation*, *28*(2), 2013, 154-169.

[13] Y.J. Yin, D. Xu, X.G. Wang, M.R. Bai, Detection and tracking strategies for autonomous aerial refueling tasks based on monocular vision, *International Journal of Advanced Robotic Systems*, *11*(97), 2014, 1-12.

[14] J.S. Kim, H.W. Kim, and I.S. Kweon, A Camera Calibration Method Using Concentric Circles for Vision Applications, *ACCV2002, Melbourne, Australia*, 2002.

[15] Z. Chen, J. Huang, A Vision-Based Method for the Circle Pose Determination With a Direct Geometric Interpretation, *IEEE Transactions on Robotics and Automation*, *15*(6), 1999, 1135-1140.

[16] J.S. Kim; P. Gurdjos and I.S. Kweon, Geometric and Algebraic Constraints of Projected Concentric Circles and Their Applications to Camera Calibration, *IEEE Transactions on Pattern Analysis and Machine Intelligence*, *27*(4), 2005, 637-642.

[17] C.P. Lu, G.D. Hager, E. Mjolsness, Fast and globally convergent pose estimation from video images, *IEEE Transactions on Pattern Analysis and Machine Intelligence*, *22*(6), 2000, 610-622.

[18] C. Martinez, L. Mejias, P. Campoy, A multiresolution image alignment technique based on direct

methods for pose estimation of aerial vehicles, *International Conference on Digital Image Computing Techniques and Applications*, 2011, 542-548.

[19] B. Yan, B. Wang, Y. Li, Optimal ellipse fitting method based on least-square principle, *Journal of Beijing University of Aeronautics and Astronautics*, *34*(3), 2008, 295.

[20] S. Dasgupta, P.M. Long, Performance guarantees for hierarchical clustering, *Journal of Computer and System Sciences*, *70*(4), 2005, 555-569.

[21] L.F. Li, Z.R. Feng, K.L. He, An improved algorithm for ellipse detection based on randomized Hough transform, *Pattern Recognition and Artificial Intelligence*, *18*(4), 2005, 459-464.

[22] F. Mai, Y.S. Hung, H. Zhong, et al, A hierarchical approach for fast and robust ellipse extraction. *Pattern Recognition*, *41*(8), 2008, 2512-2524.

Biographies

Wenqi Wu received his B.Sc. degree in electronic information engineering from North China University of Technology, Beijing, China, in 2013. He is currently a PhD student in the Research Center of Precision Sensing and Control, Institute of Automation, Chinese Academy of Sciences, Beijing, China. His current research interests include target detection, computer vision and machine learning.

Xingang Wang received the B.Sc. from Tianjin University, Tianjin, China, in 1995 and the Ph.D. degree from Changchun Institute of Optics, Fine Mechanics and Physics, Chinese Academy of Sciences, Changchun, China, in 2002. He is currently a Professor in the Research Center of Precision Sensing and Control, Institute of Automation, Chinese Academy of Sciences. His research interests include image processing and machine learning.

De Xu (M’05 – SM’09) received the B.Sc. and M.Sc. degrees from Shandong University of Technology, Jinan, China, in 1985 and 1990, respectively, and the Ph.D. degree from Zhejiang University, Hangzhou, China, in 2001, all in control science and engineering. Since 2001, he has been with the Institute of Automation, Chinese Academy of Sciences (IACAS), Beijing, China, where he is currently a Professor in the Research Center of Precision Sensing and Control. His current research interests include robotics and automation such as visual measurement, visual control, intelligent control, welding seam tracking, visual positioning, microscopic vision, micro-assembly.

Yingjie Yin received his B.Sc. degree in control science and engineering from Ocean University of China, Qingdao, China, in 2011. He is currently a PhD student in the Research Center of Precision Sensing and Control, Institute of Automation, Chinese Academy of Sciences, Beijing, China. His current research interests include target tracking, computer vision and machine learning.